

Liquid Rope Lissajous Patterns

Annemarie Aarts, Vivi Andasari, and Stef van Eijndhoven

Annemarie Aarts is Assistant Professor of Industrial Mathematics at the Technische Universiteit Eindhoven, The Netherlands. Her e-mail address is a.c.t.aarts@tue.nl.

Vivi Andasari is Ph.D. student at the University of Dundee, Scotland.

Stef van Eijndhoven is Associate Professor of Industrial Mathematics at the Technische Universiteit Eindhoven, The Netherlands, and director of the post-master study program Mathematics for Industry. His e-mail address is s.j.l.v.eijndhoven@tue.nl.

ABSTRACT

This paper presents evidence that the patterns formed by a viscous filament falling onto a moving belt can be described by Lissajous figures.

ACKNOWLEDGMENT

The authors would like to thank Marc Berkhoff and Frans van Vliet from Colbond B.V., the Netherlands, for the experiments and helpful discussions.

1. INTRODUCTION

Jules Antoine Lissajous (1822-1880) is known to students in physics and electrical engineering from the "Lissajous Figures", patterns formed when two oscillations along perpendicular lines are superimposed. In 1855, Lissajous devised a simple optical method for studying compound oscillations. To each of two vibrating objects he attached a small mirror and aimed a beam of light at one of the mirrors. The beam was reflected to the other mirror and from that second mirror to a screen, where it formed a two-dimensional pattern. Thus, Lissajous built a forerunner of the modern oscilloscope. By the way, Lissajous figures were investigated before by Nathaniel Bowditch (1773-1838), who produced them in 1815 with a compound pendulum.

Each oscillation is mathematically described by a simple harmonic motion, such as a sinusoid,

$$(1) \quad \begin{aligned} x_L(t) &= A_x \sin(\omega_x t + \varphi_x), \\ y_L(t) &= A_y \sin(\omega_y t + \varphi_y), \end{aligned}$$

where the independent variable t is time, the parameters A_x and A_y are amplitudes, ω_x and ω_y are the radians frequencies, and φ_x and φ_y phases. The compound oscillation is represented by the curve $(x_L(t), y_L(t))$, $t \geq 0$; the curve describes a pattern bound by the sides of the rectangle $-A_x \leq x \leq A_x$, $-A_y \leq y \leq A_y$ in the (x, y) -plane. The pattern shows a periodic curve only if the ratio of the frequencies ω_x/ω_y is rational. If ω_x/ω_y is irrational a tedious mathematical proof will show that as time tends to infinity the curve gradually fills the rectangle densely. Yet, the curve is not rectangle filling (c.f. [2]); given $x^* \in [-A_x, A_x]$ the vertical line segment (x^*, y) , $y \in [-A_y, A_y]$ is visited only a countably infinite number of times, while the cardinality of the line segment is not equal to the cardinality of the set of natural numbers according to Cantor.

Choices of phases and frequencies result in types of Lissajous figures. For instance, for $\omega_x = \omega_y$

and $\varphi_x = \varphi_y$ the curve follows the diagonal of the rectangle

$$(2) \quad y = \frac{A_y}{A_x} x, \quad -A_x \leq x \leq A_x;$$

for $\omega_x = \omega_y$ and $\varphi_y - \varphi_x = \frac{1}{2}\pi$ the ellipse

$$(3) \quad \left(\frac{x}{A_x}\right)^2 + \left(\frac{y}{A_y}\right)^2 = 1;$$

and for $\omega_y = 2\omega_x$ and $\varphi_y - \varphi_x = \frac{1}{2}\pi$ the parabola

$$(4) \quad \frac{y}{A_y} = 1 - 2\left(\frac{x}{A_x}\right)^2, \quad -A_x \leq x \leq A_x,$$

using the identity $\cos 2\alpha = 1 - 2\sin^2 \alpha$. In all cases the period equals $T = 2\pi/\omega_x$. An extensive overview of the various Lissajous figures is presented in [1].

Patterns very similar to the Lissajous figures can be obtained from an experiment that is even simpler than the one devised by Lissajous. What is needed is syrup, a spoon, and a plateau that can move with a constant speed in a specified direction. Take the spoon, fill it with syrup, and let the syrup fall freely from the spoon onto the moving plateau from a height of 10 cm say. The syrup will form a "liquid rope" that having dropped on the moving surface shows a stitching pattern. The shape of the pattern depends on the fall height and the velocity of the moving plateau. In case the plateau is kept still the jet of syrup shows a coiling pattern.

Studies have been performed on these coiling phenomena where the falling syrup is considered a viscous fluid filament and the moving plateau replaced by a belt with a well-controlled velocity, c.f. [3], [4], [5], [6], [7]. Through experiments or simulations based on a mathematical model, the relationship between the process parameters, – fall height, initial speed of the filament, and velocity of the belt –, the material parameters of the fluid, – viscosity and mass density –, and the shape of the pattern formed at the belt. For that a description, in mathematical terms, of these patterns is needed. To be specific, if we let x be the direction in which the belt moves and y the direction perpendicular to x , we write the pattern formed by the dropping filament as planar curve

$$(5) \quad \begin{aligned} x(t) &= V_{\text{belt}} t + x_C(t), \\ y(t) &= y_C(t), \end{aligned}$$

where t denotes time and V_{belt} the velocity of the belt.

As the main result of this paper we present convincing evidence that the curve $(x_C(t), y_C(t))$,

$t \geq 0$, is a Lissajous curve, where both $x_C(t)$ and $y_C(t)$ are simple sinusoids according to Equation (1). We show the effects of changing the velocity V_{belt} , radians frequencies ω_x and ω_y , phases φ_x and φ_y , and amplitudes A_x and A_y on the patterns obtained from this mathematical representation. Accepting the hypothesis that the patterns at the belt can be described by Lissajous figures based on simple sinusoids, the complex mathematical model [5] that describes the dynamic behavior of the falling filament onto a moving surface, should focus on determining the fundamental frequencies, amplitudes and phases that fit the desired pattern. Thus, the complexity in the analysis of the mathematical model can be reduced greatly.

2. EXPERIMENTAL SET-UP

For the validation of our hypothesis we performed experiments, as shown in Figure 1. These experiments have been carried out to get insight into a production process of polymer mats that are used for erosion protection. Such a polymer mat consists of polymer filaments entangled together, forming a three-dimensional structure; a sample is presented in Figure 2. For the production of the mat use is made of the coiling phenomena of polymer filaments. In the production process a large number of polymer filaments fall parallel onto a moving surface. To optimize the production process simulations are performed to determine the relation between process parameters and material parameters, on one hand, and the coiling parameters, frequency and amplitude, on the other hand. As in any production process the aim is to increase throughput. But, at the same time, the product must meet certain quality specifications, that are formulated in terms of thickness of the polymer filaments when they reach the surface and diameter of the coils that are formed. Thus, the simulations should reveal optimal process parameters and material parameters.

In the experimental set-up a molten polymer filament, pushed through a spinneret hole falls onto a moving belt with a well-controlled speed V_{belt} from a certain height; c.f. Figure 1. Samples of the patterns formed by the filament at the belt surface with a length of 20 cm are taken; c.f. Figure 3. For each of these samples the corresponding amplitudes, frequencies, and phases are determined. A time-tuning step is performed and

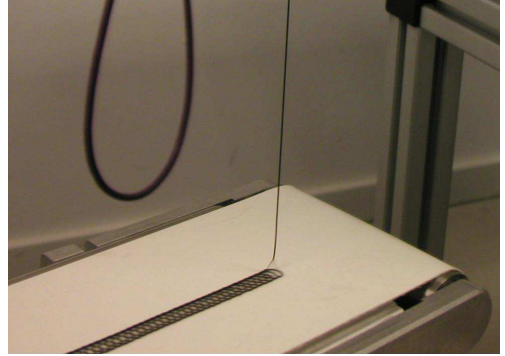


FIGURE 1. The experimental set-up, in which a molten polymer filament falls onto a moving belt.

the resulting model pattern

$$(6) \quad \begin{aligned} x(t) &= V_{\text{belt}} t + A_x \sin(\omega_x t + \varphi_x) \\ y(t) &= A_y \sin(\omega_y t + \varphi_y), \end{aligned}$$

is, on scale, compared with a digital picture of the corresponding experimentally obtained pattern.



FIGURE 2. Sample of a polymer mat that is produced by making use of coiling of polymer filaments that fall onto a moving surface.

In Figures 3 and 4 the samples obtained from the experiments are shown. Each sample, being laid out on the moving belt in a certain pattern, corresponds to a certain speed of the belt. The fall height in Figure 4 is taken $7/3$ times larger than that of Figure 3. As a result, the filaments of Figure 4 reached during their fall a larger speed than those of Figure 3. In Figure 3 we see that sample 1, taken at a relatively high belt speed, is just a straight filament. Reducing the belt speed changes the pattern to meandering (samples 2-5), and reducing the belt speed even further, the pattern again changes to filaments being laid out in coils (samples 6 and 7). For a larger fall height we observe a different tendency, c.f. Figure 4; at

large belt speeds the samples show a figure-of-eight pattern (samples 8-11) and for reduced belt speeds a coiling pattern (samples 12-14).

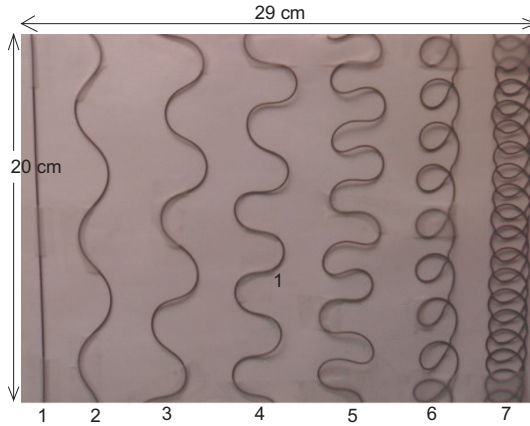


FIGURE 3. Polymer samples from experiments, falling from a relatively small height, for different belt speed V_{belt} : (1) $V_{\text{belt}} = 7.3$ m/min, (2) $V_{\text{belt}} = 6.3$ m/min, (3) $V_{\text{belt}} = 5.3$ m/min, (4) $V_{\text{belt}} = 4.3$ m/min, (5) $V_{\text{belt}} = 3.3$ m/min, (6) $V_{\text{belt}} = 2.3$ m/min, and (7) $V_{\text{belt}} = 1.3$ m/min.

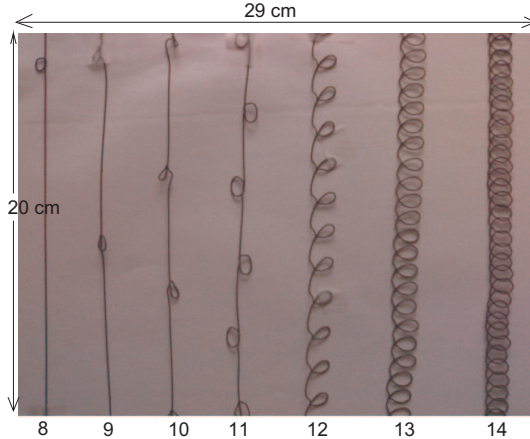


FIGURE 4. Polymer samples from experiments, falling from a relatively large height, for different belt speed V_{belt} : (8) $V_{\text{belt}} = 14.6$ m/min, (9) $V_{\text{belt}} = 12.6$ m/min, (10) $V_{\text{belt}} = 10.6$ m/min, (11) $V_{\text{belt}} = 8.6$ m/min, (12) $V_{\text{belt}} = 5.6$ m/min, (13) $V_{\text{belt}} = 3.6$ m/min, and (14) $V_{\text{belt}} = 2.3$ m/min.

We mathematically describe the different patterns obtained from the experiments by Equation (6). The belt speed we set to the actual one

used in the experiments and we determine amplitudes A_x and A_y , frequencies $f_x = \omega_x/(2\pi)$ and $f_y = \omega_y/(2\pi)$, and phases φ_x and φ_y , according to the following rules of thumb:

- The phase φ_y we set to zero.
- The amplitude A_y is half the width of the samples.
- For the frequencies we distinguish a meandering pattern, a coiling pattern, and a figure-of-eight pattern:

In case of a meandering pattern the number N_y of crossings through the imaginary line " $y = 0$ " is counted for the sample length L . The time t_L needed to form a sample of length L equals $t_L = L/V_{\text{belt}}$ so that the frequency f_y for a meandering pattern is determined from $f_y = \frac{1}{2}N_y/t_L = N_y V_{\text{belt}}/(2L)$. To get a meandering pattern the ratio $f_x : f_y$ equals 2 : 1, since then the wave pattern induced by the y -motion is not changed. To widen the waves of the meanders and keep them symmetric the x -motion has to be precisely in anti-phase with the y -motion, i.e., $\varphi_x = \pi$. The amplitude A_x is determined by a trial and error tuning.

In case of coiling and figure-of-eight patterns the number of coils, N_{coils} , in the patterns are counted for the given sample length L . In each coil the x -motion changes its direction twice, i.e., once from going along with the belt motion to its opposite direction and once to the belt motion direction back again. Thus, within each period $T = 1/f_x$ one coil being formed, the frequency f_x for a coiling or figure-of-eight pattern satisfies $f_x = N_{\text{coils}}/t_L = N_{\text{coils}} V_{\text{belt}}/L$. For a coiling pattern, in forming a coil the filament passes the imaginary line " $y = 0$ " twice, so that $f_y = f_x$. For a figure-of-eight pattern, however, in forming a coil, the filament passes the imaginary line " $y = 0$ " precisely 3 times, so that the ratio $f_x : f_y$ equals 2 : 3 for a figure-of-eight pattern. The skewness of the coils determines the phase φ_x . Finally, for the coiling and figure-of-eight patterns, in each period of length $T = 1/f_x$ there must be two moments of time at which the derivative dx/dt is zero. Using Equation (6), the equation

$$(7) \quad V_{\text{belt}} + \omega_x A_x \cos(\omega_x t + \varphi_x) = 0$$

must have two zeroes in the time interval $0 \leq t \leq 1/f_x$, and, thus, A_x satisfies

$$(8) \quad A_x \geq \frac{V_{\text{belt}}}{\omega_x}$$

in case of a coiling or figure-of-eight pattern.

In Tables 1, 2, and 3 we present the values of A_x , A_y , f_x , f_y and φ_x for the meandering, coiling, and figure-of-eight patterns, and in Figures 5, 6, and 7 the graphs of the corresponding model patterns that can be compared with Figure 3, samples 1-5, Figures 3 and 4, samples 6, 7, 12-14, and Figure 4, samples 8-11, respectively.

sample	V_{belt} [$\frac{\text{m}}{\text{min}}$]	A_y [cm]	f_y [Hz]	A_x [cm]	f_x [Hz]	φ_x [$^\circ$]
2	6.3	0.9	1.5	0.1	3.0	180
3	5.3	1.2	1.6	0.1	3.2	180
4	4.3	1.5	1.6	0.15	3.2	180
5	3.3	1.6	1.65	0.2	3.3	160

TABLE 1. Amplitudes, frequencies and phases for the meandering patterns of Figure 3. The frequency ratio is $f_x = 2f_y$.

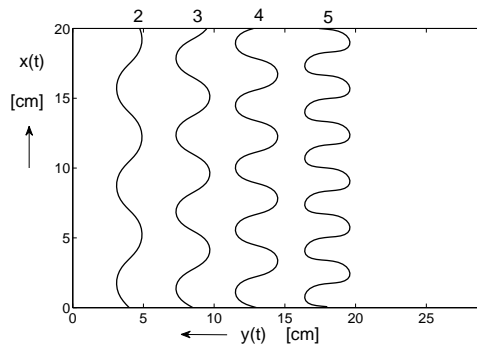


FIGURE 5. Meandering patterns obtained by use of Equation (6) with parameter values of Table 1, corresponding to the meandering samples of Figure 3 obtained from experiments.

sample	V_{belt} [$\frac{\text{m}}{\text{min}}$]	A_y [cm]	f_y [Hz]	A_x [cm]	f_x [Hz]	φ_x [$^\circ$]
6	2.3	1.1	1.7	1.3	1.7	115
7	1.3	1.2	1.7	1.4	1.7	90
12	5.6	0.7	5.4	1.0	5.4	-120
13	3.6	0.8	6.4	0.6	6.4	-100
14	2.6	0.7	6.8	0.6	6.8	-90

TABLE 2. Amplitudes, frequencies and phases for the coiling patterns of Figures 3 and 4. The frequency ratio is $f_x = f_y$.

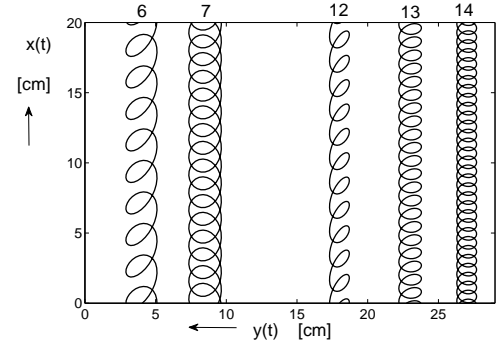


FIGURE 6. Coiling patterns obtained by use of Equation (6) with parameter values of Table 2, corresponding to the coiling samples of Figures 3 and 4 obtained from experiments.

sample	V_{belt} [$\frac{\text{m}}{\text{min}}$]	A_y [cm]	f_y [Hz]	A_x [cm]	f_x [Hz]	φ_x [$^\circ$]
8	14.6	0.3	1.6	4.7	1.07	0
9	12.6	0.3	2.9	2.6	1.93	0
10	10.6	0.3	4.0	1.8	2.67	0
11	8.6	0.5	5.4	1.3	3.60	0

TABLE 3. Amplitudes, frequencies and phases for the figure-of-eight patterns of Figure 4. The frequency ratio is $3f_x = 2f_y$.

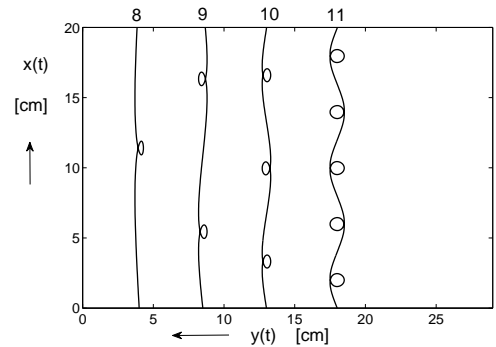


FIGURE 7. Figure-of-eight patterns obtained by use of Equation (6) with parameter values of Table 3, corresponding to the figure-of-eight samples of Figure 4 obtained from experiments.

In Figures 8, 9, and 10 we present the Lissajous figures, $(x_C(t), y_C(t))$, corresponding to the patterns presented in Figure 5, 6, and 7, respectively.

We close the paper with an artificial pattern plotted in Figure 11 that follows the model (6), but was, up to now, not experimentally observed.

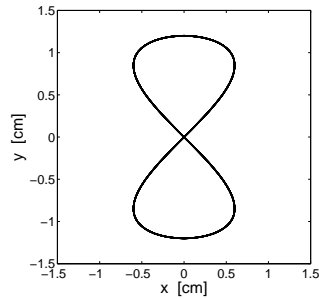


FIGURE 8. Lissajous figure ($V_{\text{belt}} = 0$) that corresponds to the meandering patterns ($f_x = 2f_y$) of Figure 5. Here, $A_y = 1.2$ cm, $A_x = 0.6$ cm, $\varphi_y = 0$, $\varphi_x = \pi$.

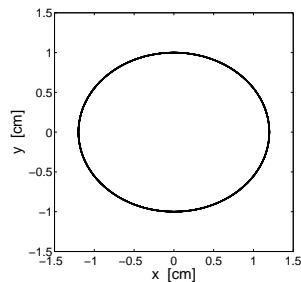


FIGURE 9. Lissajous figure ($V_{\text{belt}} = 0$) that corresponds to the coiling patterns ($f_x = f_y$) of Figure 6. Here, $A_y = 1.0$ cm, $A_x = 1.2$ cm, $\varphi_y = 0$, $\varphi_x = \pi/2$.

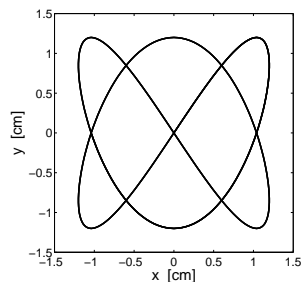


FIGURE 10. Lissajous figure ($V_{\text{belt}} = 0$) that corresponds to the figure-of-eight patterns ($3f_x = 2f_y$) of Figure 7. Here, $A_y = 1.2$ cm, $A_x = 1.2$ cm, $\varphi_y = \varphi_x = 0$.

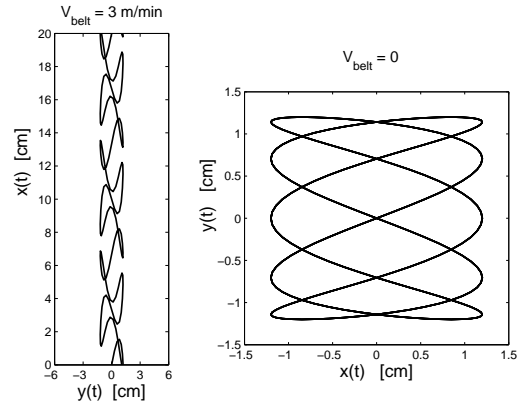


FIGURE 11. Artificial pattern (left picture, $V_{\text{belt}} = 3$ m/min) and the corresponding Lissajous figure (right picture, $V_{\text{belt}} = 0$), for $f_x/f_y = 5/2$, $f_y = 1.5$ Hz, $A_y = A_x = 1.2$ cm, $\varphi_y = \varphi_x = 0$.

3. CONCLUSION

In this paper we validate the hypothesis that the pattern formed by a falling viscous filament on a moving flat surface is essentially a Lissajous figure. We describe how model parameters, amplitudes, frequencies, and phases, can be derived from a sample pattern. We perform the actual validation on the basis of 16 samples obtained from an experiment carried out in a well-controlled laboratory environment. Thus, simple mathematics is capable of describing relevant aspects of complicated physical processes

REFERENCES

- [1] M.S Wu and W.H. Tsai, "Corrections for Lissajous figures in books", *American Journal of Physics*, Vol. 52 (1984) pp. 657-658.
- [2] J.M. Diaz de la Cruz Cano and J.J. Scala Estalella, "Lissajous curves do not fill a rectangular area" *American Journal of Physics*, Vol. 64 (1996) pp. 499-500.
- [3] S. Chiu-Webster and J.R. Lister, "The Fall of a Viscous Thread onto a Moving Surface: a 'Fluid-Mechanical Sewing Machine'", *Journal of Fluid Mechanics*, Vol. 569 (2006), pp. 89-111.
- [4] N.M. Ribe, "Coiling of Viscous Jets", *Proceedings of the Royal Society of London A*, Vol. 460 (2004), pp. 3223-3239.
- [5] N.M. Ribe, M. Habibi, and D. Bonn, "Stability of Liquid Rope Coiling", *Physics of Fluids*, Vol. 18

(2006).

- [6] N.M. Ribe, H.E. Huppert, M.A. Hallworth, M. Habibi, and D. Bonn, "Multiple Coexisting States of Liquid Rope Coiling", *Journal of Fluid Mechanics*, Vol. 555 (2006), pp. 275-297.

- [7] N.M. Ribe, J.R. Lister, and S. Chiu-Webster, "Stability of a Dragged Viscous Thread: Onset of "Stitching" in a Fluid-Mechanical "Sewing Machine"", *Physics of Fluids*, Vol. 18 (2006).